MRI Temperature Mapping and Determination of Liquid-particulate Heat Transfer Coefficient in an Ohmically Heated Food System

X. YE, R. RUAN, P. CHEN, C. DOONA, AND I.A. TAUB

ABSTRACT: Real-time temperature maps of ohmically heated liquid-particulate mixtures were acquired using the Proton Resonance Frequency (PRF) shift method incorporated into a fast Magnetic Resonance Imaging (MRI). Noise in the MRI images induced by the electrical heating power was eliminated by a post-processing algorithm of the PRF shift method and correction phase images. The time-dependent interface heat transfer coefficients (h_{fp}) were determined during the holding period using the MRI temperature maps and numerical solutions to the Fourier's 2nd law. The calculated values of h_{fp} range from 30 to 105 W/m^2·K, consistent with literature values for natural convection. These results provide crucial data for understanding the ohmic heating process.

Keywords: MRI, temperature mapping, PRF shift, ohmic heating, heat transfer coefficient

Introduction

THE UNIQUE INTERNAL HEAT GENERATION OF ohmic heating shows promise for quality preparation of liquid-particulate foods. However, this uniqueness also makes difficulty for the understanding of the ohmic heating process. The commercialization of the ohmic heating technology depends in part on the development of adequate safety and quality assurance protocols in order to obtain an approved filing of the process with the FDA. One critical component in understanding the process lies in the development of mathematical models, which can then be used to simulate various effects of critical factors, such as the electrical conductivity of the materials and the liquid viscosity, and to guide the process design and quality control. Currently, existing models are limited to specific conditions, due to a lack of the understanding of the temperature distribution and thermal interactions within the system. In the current models (Fryer and others 1993; Sastry and Li 1996; Orangi and others 1998), the effect of convection at the liquid-particulate interface is over-simplified, but the accurate determination of the fluid-particulate convective heat transfer coefficient has been a challenge faced in the processing of foods containing particulates (Bhamidipati and others 1995). This heat transfer coefficient (h_{fp}) is often calculated with an empirical correlation between dimensionless numbers. This approach is obviously restricted to the range of conditions for which the correlation was determined and to the design characteristics of the heating system (Ananthesweran and others 1985; Merson and Stoforos 1990). Other methods for the calculation of the heat transfer coefficient involve fitting the process equations to the experimental data, with h_{fp} being the only factor to be determined by regression. Previous research in mass transfer (Azevedo and others 1998) concluded with statistical certainty that if both the internal and external heat transfer parameters (both h_{fp} and the thermal diffusivity a) are determined jointly by experimental data, the errors will likely be very large and a strong collinearity between the parameters will prevent a minimally reasonable estimate of the parameters. An exception may occur in a relatively narrow intermediate range of the Biot number, where the internal and external resistance is balanced. Therefore, the internal heat transfer must be well determined by previous data before the calculation of the external coefficient.

The application of Magnetic Resonance Imaging (MRI) techniques in food engineering research enabled noninvasive spatial temperature mapping (Schrader and others 1992; Sun and others 1994; Hulbert and others 1995), providing a powerful tool to study heat transfer in food and biological systems. When MRI techniques are applied to the ohmic heating process, 2 concerns were raised by peers: (1) long data acquisition times make the techniques unsuitable for a dynamic process like ohmic heating; (2) the electrical heating power has to be interrupted during the data acquisition due to its interference with the magnetic field, otherwise inaccurate temperature maps will be obtained. Ye and others (2002) acquired temperature maps of ohmically heated whey gel and brine using the proton resonance frequency (PRF) shift method incorporated into MRI phase imaging. The fast imaging sequence in the study rendered temperature maps with a spatial resolution of 0.94 millimeters and a temporal resolution of 0.64 s. However, the power was still disconnected for about 3 s during data acquisitions.

The objectives of this work are: (1) to obtain 2-dimensional temperature maps of ohmically heated food materials using the PRF shift method without disconnecting the electrical heating power; (2) to estimate the fluid-particulate heat transfer coefficient in a static ohmic heater during the holding period from the temperature maps.

Materials and Methods

Materials

The experimental set-up is shown schematically in Figure 1. Two sample systems were prepared, with each consisting of a cylindrical heating device, a cylindrical potato particle, and a salt solution with sodium carboxymethylcellulose (CMC). The ohmic heating device of sample nr 1 consisted of a Plexiglas vessel with an inner dia of 43 mm and a nylon stopper at each end. A 40-mm dia stainless steel electrode was fixed to each of the stoppers and connected to the power supply. The distance between the 2 electrodes was 305 mm. A small hole was drilled in the vessel for injection of the fluid and for pressure release during heating.

© 2003 Institute of Food Technologists
Further reproduction prohibited without permission

The heating vessel of sample nr 2 was made of a clear PVC tube with an inner dia of 63.5 mm. A 60-mm dia stainless steel electrode was fixed to each of the nylon stoppers of sample nr 2. All other dimensions were the same as sample nr 1.

Salt solutions with CMC were prepared overnight using a hot plate magnetic stirrer. The CMC and NaCl powders were added gradually to a measured amount of water and heated while being continuously stirred to avoid clumping. For sample nr 1, the concentration of NaCl and CMC was 0.2% (w/w) and 1.2% (w/w), respectively. For sample nr 2, the concentration of NaCl and CMC was 0.5% (w/w) and 0.7% (w/w), respectively. These levels of salt and CMC were chosen in order to see their effects on the differential heating between the liquid and the solid phases and on the interface heat transfer. Two cylindrical potato particles were freshly cut from Russet potatoes immediately before the experiment and put in the middle of each heating vessel. The dimension of the potato particle was 70 mm (length) × 22 mm (dia) for sample nr 1 and 75 mm (length) × 25 mm (dia) for sample nr 2. The fluid was then injected through the small hole into the vessel. Due to the higher density of the solutions, the potato particles floated on the surface of the fluids. The application of an AC power supply with a constant voltage of 120 V and a frequency of 60 Hz ohmically heated the food systems.

MR Imaging

A volume birdcage radio frequency (RF) coil that fitted the configuration of each heating vessel was used as both an RF transmitter and MR signal receiver. A thin tube containing an agar gel was inserted between the ohmic heating vessel and the RF coil. The tube was thermally insulated by Styrofoam so that the phase change of MRI images induced by sources other than the temperature change will be revealed by the phase images in the agar gel. Two-dimensional MR imaging was performed using a 4.7 Tesla SISCO scanner (Varian, Palo Alto, Calif., U.S.A.) with a 330 mm dia bore at the Center for Magnetic Resonance Research at the Univ. of Minnesota. The PRF shift method was incorporated into a Fast Low Angle SHot (FLASH) sequence (Ishihara and others 1995) to achieve a rapid image acquisition. This method exploits the temperature dependence of the proton resonance frequency (PRF) shift and the PRF shift can be manifested through MR phase images. A detailed review about the PRF shift method can be found in Ye and others (2002). The schematic diagram of the imaging sequence used for this study is shown in Figure 2.

Transverse images were obtained using the following imaging parameters: repetition time TR = 10 msec; echo time TE = 4.6 msec; flip angle FA ≅ 12°; slice thickness = 3 mm; and image matrix size = 64 × 64. The only difference between the imaging sequences applied to the 2 samples was the field of view (FOV), which was 60 mm × 60 mm for sample nr 1 and 80 mm × 80 mm for sample nr 2. Therefore, the temporal resolution (data acquisition time for one temperature map) was 0.64 s for both samples. The spatial resolution of the temperature maps was 0.94 mm for sample nr 1 and 1.25 mm for sample nr 2.

The reference images were scanned after the sample systems had equilibrated to room temperature (20.5 °C). Three images were obtained at room temperature and their phase images were averaged and used as the reference phase image. For sample nr 1, the images were acquired, without disconnecting the electrical power, every 5 min until 55 min after switch-on of the heating power. Then the ohmic heating was stopped to simulate a holding period. MRI images were also acquired every 5 min until 50 min after the heating was stopped. For sample nr 2, data were collected, without disconnecting the power, at 5, 10, 15, 20, 23, 25, 27, and 29 min after the switch-on of the power. The heating was stopped at the last point, again, to simulate a holding period. During the holding period, sample nr 2 was imaged every 2.5 min until 50 min after the heating was stopped.

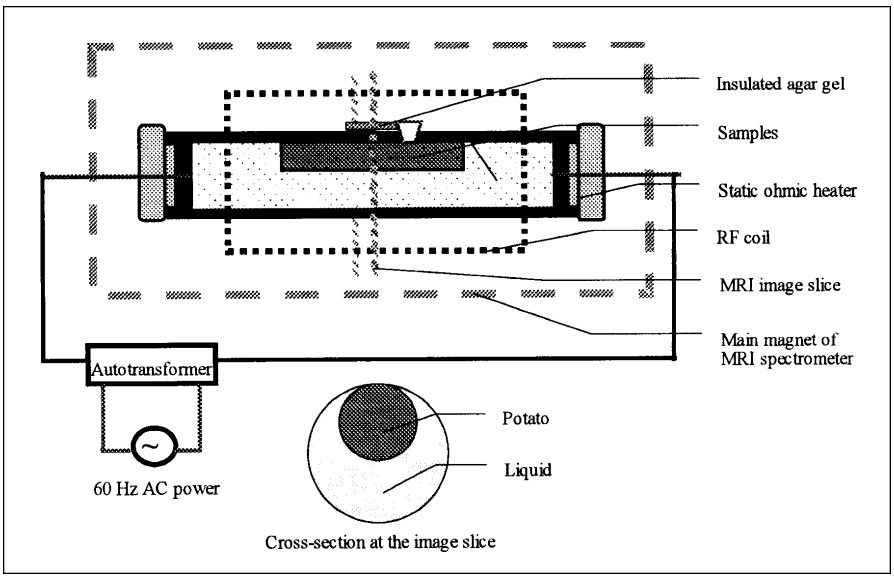

Figure 1—Schematic diagram of experimental set-up

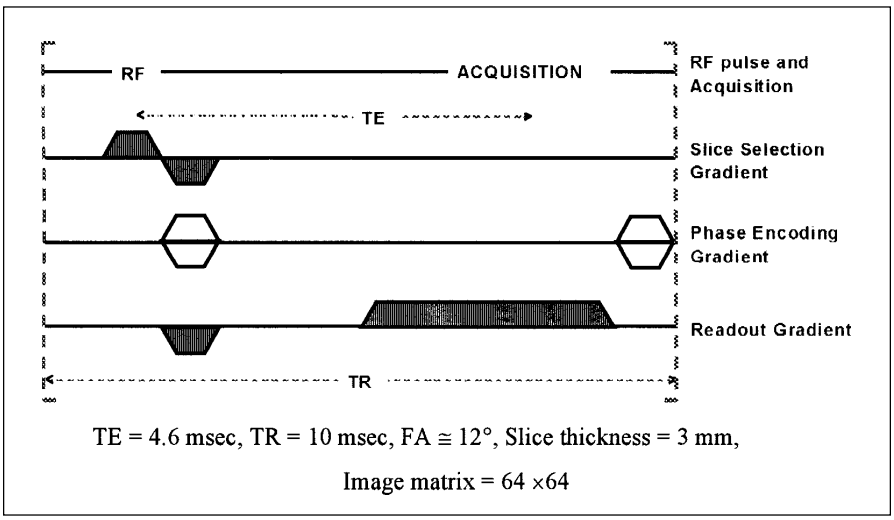

Figure 2—Schematic diagram of the imaging sequence

JFS is available in searchable form at *www.ift.org*

Processing of the temperature maps

The temperature sensitivity of the PRF was first observed by Hindman in 1966 (Hindman 1966). The fractional change of water proton resonance frequency ($\Delta\omega/\omega$) with temperature is defined as δ. It is also referred as proton chemical shift or PRF shift. Mathematically,

$$\frac{\Delta\omega}{\omega} = \delta \cdot \Delta T \quad (1)$$

where ΔT is the temperature change. Experimentally, d has been determined as –0.01 ppm/°C in water (Hindman 1966). It is generally assumed that the water PRF shift to lower frequency with higher temperature is caused by rupture, stretching, or a small amount of bending of the hydrogen bonds (Muller and Reiter 1965; Hindman 1966). This means a reduction in the average degree of association of water molecules, and these shifts are evidence of an increased average shielding constant of the protons (Ishihara and others 1995). The proton resonance frequency shift imaged at a static field strength B_0 after having undergone a temperature change of ΔT is:

$$\Delta\omega = \delta \cdot \gamma \cdot B_0 \cdot \Delta T \quad (2)$$

where γ is the gyromagnetic ratio of the proton. This frequency change manifests as a phase change when imaged with a gradient-echo sequence having an echo time *TE*. This phase change $\Delta\phi$ can be expressed as:

$$\Delta\Phi = \delta \cdot \gamma \cdot B_0 \cdot \Delta T \cdot TE \quad (3)$$

The phase image $\phi(x,y)$ can be calculated from the acquired complex data of the MR image using Eq. 4:

$$\Phi(x,y) = \arctan\left[\frac{\mathrm{Im}(x,y)}{\mathrm{Re}(x,y)}\right] \quad (4)$$

where *Im(x,y)* and *Re(x,y)* are the imaginary and real part of the complex MRI data, and *x* and *y* denote the image pixel numbers.

To use the PRF shift technique to map temperature, a reference phase image is first acquired at a known temperature, and that reference is subtracted from subsequent phase images taken as the temperature changes. Temperature maps are obtained based on the reference temperature and the echo time TE of the image sequence according to Eq. 3.

All of the MR image reconstruction and post-processing were performed off-line on a SUN Ultra 10 workstation (SUN Microsystems, Mountain View, Calif., U.S.A.) and a PC computer. The processing details can be found in Ye and others (2002). Those experiments entailed disconnecting the electrical power during imaging. One improvement in the present experiments is that the heating power was not disconnected, as shown below. Although the built-in filter of the imager successfully eliminated most of the noise due to the electrical power, there were still some stripes of noise on the regular MR images. After processing the data, no obvious noise could be discerned in the phase difference images and the temperature maps because the PRF shift method calculates the relative temperature from the phase difference and the noise cancelled when the subsequent phase image was subtracted. The electrical current passing through the food systems changed due to the change in electrical conductivity of the food materials with temperature. This change might have induced a shift in the local magnetic field (B_0), which in turn would affect phase images. The agar gel was used as a reference to compensate for the phase change due to the B_0 shift. Because the tube was thermally and electrically insulated, any change of phase induced by a source other than temperature change would be reflected in a phase change in the agar gel. Therefore, the phase change in the agar gel was subtracted from the corresponding phase difference image to accurately map temperature.

Determination of the convective heat transfer coefficient

In this study, a modeling procedure with a numerical solution was used to match the calculated temperature distribution with that measured with MRI. Such a noninvasive procedure together with a finite-element method is especially useful for modeling the heating of a liquid-particulate mixture with irregular particulate shapes.

To simplify the calculation, this study determined the heat transfer coefficient during only the holding period, which involved mainly natural convective heat transfer. With the knowledge of the electrical conductivity and its temperature dependence of the food materials, the procedure used in this study can be easily adapted to determine h_{fp} during the ohmic heating period. The geometry for the potato samples was drawn in MATLAB according to the corresponding MRI images. Figure 3 shows the geometry and mesh of the 2 samples used in the modeling.

The governing equation is the Fourier's second law without internal heat generation applied to the cylindrical potato particle:

$$\rho_p C_P \frac{\partial T_p}{\partial t} = \nabla \cdot (k_p \nabla T_p) \quad (5)$$

The convective heat transfer between the fluid phase and the solid phase is the required boundary condition and is given by:

$$-k_p \nabla T_p \cdot \vec{n}\big|_s = h_{fp}(T_{ps} - T_f)\big|_s \quad (6)$$

where ρ_p is the density of the potato particle, C_P is specific heat of the particle, T_p is the particle temperature that is both time and location dependent, *t* is time, k_p is the particle thermal conductivity, and T_f the fluid temperature. The subscript "*s*" in Eq. 6 stands for surface. In most cases reported in the literature, a constant fluid temperature was considered (Maesmans and others 1992). In this study, the actual time-temperature profile obtained from MRI temperature mapping was used as a time-dependent boundary condition. An exception was granted to boundary A in sample nr 2 (Figure 3) where an adiabatic condition was as-

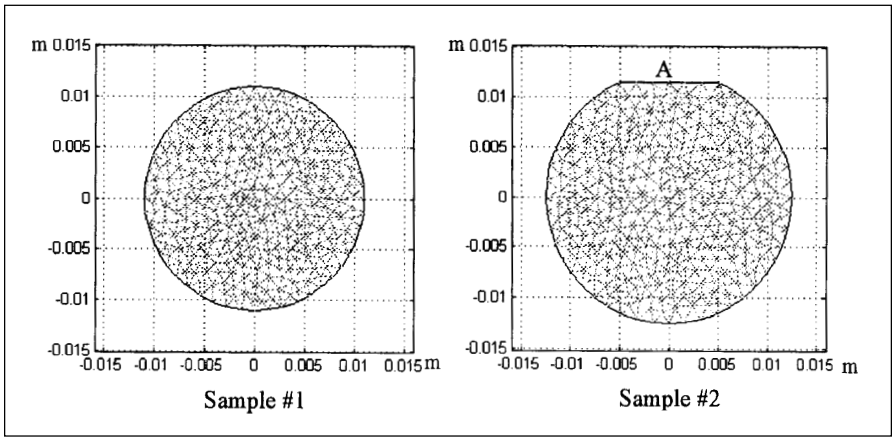

Figure 3—Geometry and mesh of the 2 potato samples in MATLAB

sumed. In sample nr 2, due to the leaking of the fluid, the top part of the potato particulate was not immersed in the fluid. Therefore, this part of the potato was cut off at the boundary A, and it was reasonable to assume an adiabatic boundary condition at A because only slow conduction heat transfer actually took place at boundary A. By varying h_{fp}, an computationally intensive optimization algorithm was employed to minimize a function $f(h_{fp})$ defined as the sum of the squared differences between the temperatures calculated by the model and those obtained with MRI temperature mapping:

$$f(h_{fp}) = \sum_{i}^{n} (T_{i_{MRI}} - T_{i_{MODEL}})^2 \qquad (7)$$

where i is an index corresponding to the pixels in the potato image. The average h_{fp} over a time period was determined as the h_{fp} value that minimized the function $f(h_{fp})$.

The partial differential Eq. 5 and 6 was solved in the PDE Toolbox (version 1.0.3) of MATLAB (version 6.0, The Mathworks, Inc. Natick, Mass., U.S.A.). The PDE Toolbox uses the finite element method to solve partial differential equations by incorporating the powerful Delaunary triangulation algorithm to generate unstructured meshes for the specified geometries, and then solves for these meshes. The time-stepping algorithms in MATLAB uses automatic time step control so that the convergence criteria (0.001 K in this study) is satisfied, but the users can specify certain times for which the solution must be calculated and stored. In this study, the model temperature at the end of each 5-min interval was calculated and stored. The results for the elements were interpolated into a finite difference scheme by using a built-in function "tri2grid" in order to be compared with the corresponding MRI temperature maps. The physical properties of the potato particles used in the calculations were: density $\rho_p = 1030$ kg/m^3; specific heat $C_p = 3795$ J/kg·K; thermal conductivity k = 0.66 W/m·K. (Gratzek and Toledo 1993; Awuah and others 1996)

Results and Discussion

MRI temperature maps

The MRI temperature maps of the samples at selected times during ohmic heating and holding period are shown in Figures 4(a) and (b). The MRI slice is 2-dimensional in the x-y plane and the temperature is projected in the z-axis to generate a 3-D image. The 64 × 64 pixels of the temperature maps show the details of the temperature distribution since every pixel represents a temperature value at that location. In addition, the maximum phase change in the agar gel is 0.0647 radians, which correspond to a temperature change of less than 1.2 °C, indicating that the effect of the B_0 shift was not significant.

Sample nr 1 had a NaCl concentration of 0.2% and the maps show that the fluid phase heated up just slightly faster than the particulate phase. Importantly, the MRI maps show that the cold spot in the potato of sample nr 1 was not located at the center. At a NaCl concentration of 0.5%, the fluid phase in sample nr 2 heated so much faster than the potato particle that the average temperature of the fluid was about 17 °C higher than that of the potato particle 25 min after switch-on of the power.

The cylindrical potato particles floated on the fluids due to their lower densities. The top edge of the particles in contact with the heating vessel wall heated slowly because of the absence of conductive fluid. This was even more obvious for sample nr 2, in which some fluid leaked out of the heating vessel. We can postulate that the electrical current density in the fluid surrounding the potato particle (Zone A, Figure 5) was higher than that in other regions (Zones B and C, Figure 5) within the system because the electrical current was "diverted" to the fluid when the fluid phase had a higher electrical conductivity than the solid phase. This resulted in a faster heating around the particle, as is evident from the first 2 temperature maps of each sample. This observation supports the application of Laplace equation to model the electric field during ohmic heating, as suggested by de Alwis and Fryer (1990):

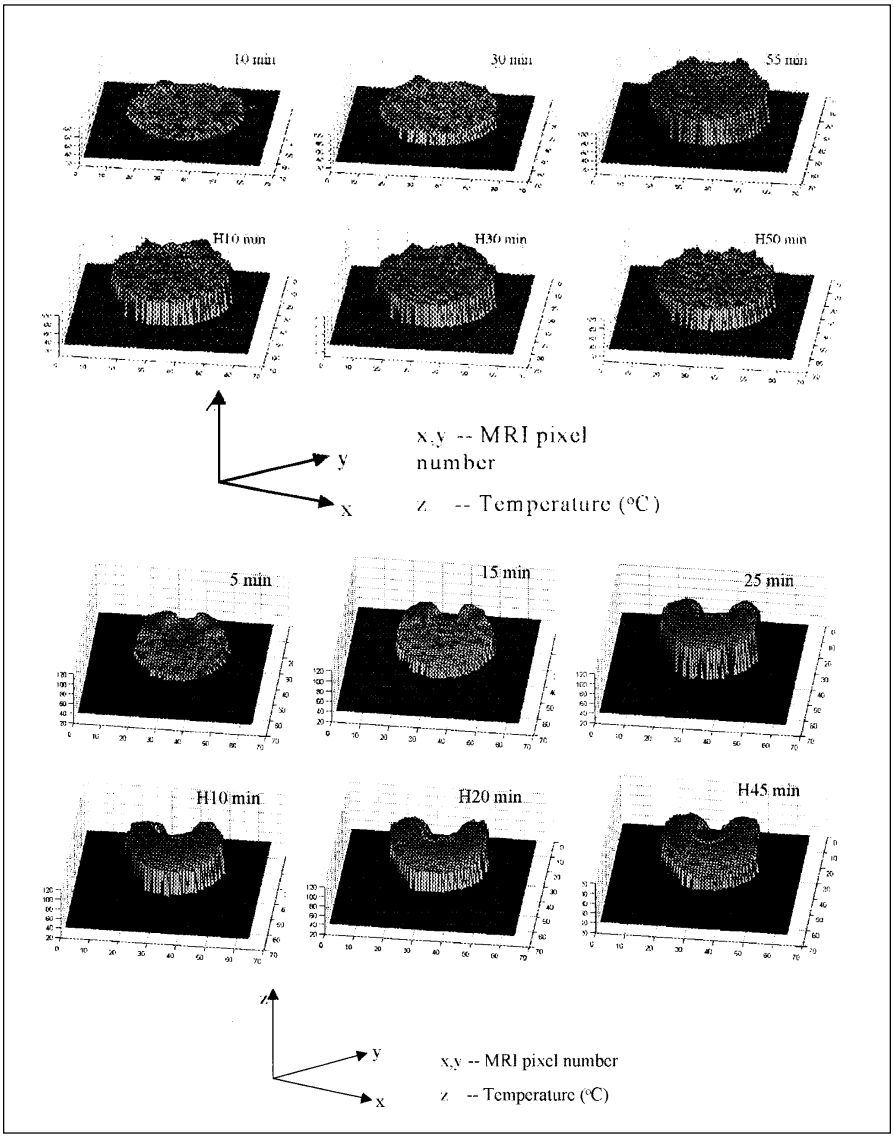

Figure 4—(a, top) Temperature maps of sample nr 1 at selected time points. 'H' denotes holding period; (b, bottom) temperature maps of sample nr 2 at selected time points. 'H' denotes holding period.

JFS is available in searchable form at www.ift.org

$$\nabla \cdot [\sigma_i(T)\nabla V] = 0 \quad (8)$$

where V is the applied voltage, ∇ is gradient, $\sigma_i(T)$ is electrical conductivity of phase i which can take on different values for the particulate (p) and fluid phase (f) and is a function of temperature. Laplace equation was derived from Ohm's law and the equation of continuity. It models the electrical current flow as curved lines according to the electrical conductivity distribution of the food materials; thus the electrical current will be "diverted" from the potato to the fluid if fluid phase has a higher electrical conductivity than the solid phase, resulting in a nonuniform distribution of the current density and a consequent nonuniform heating rate. A numerical simulation using Laplace equation was conducted in MATLAB for the same geometry as the experiment in the study and the result is shown in gray scale in Figure 5. The constant electrical conductivity values used in the simulation were 1.3 S/m for fluid and 0.037 S/m for potato and these values were taken from Kim and others (1996). The simulation shows that when the potato particle has a lower electrical conductivity than the fluid, there exits a high electrical density zone around the particle, consistent with the MRI temperature observations.

To be able to model an ohmic heating process, the coupled partial differential equation system of Laplace equation and the Fourier's equation with internal heat generation must be solved simultaneously. Because the 2 equations are coupled through temperature (T), it is critical to obtain values of electrical conductivity as function of temperature. Unfortunately, only sparse and inconsistent data are available in the literature for this important property. It is a great interest to investigate the electrical conductivity and its temperature dependence for the ohmic heating research. An agreement that can be found in the literature (Halden and others 1990; Palaniappan and others 1991a, b; de Alwis and Fryer 1992) is that the electrical conductivity of potato experiences a sharp upturn when the temperature of potato reaches approximately 320 K. With the increase of the sample temperature, the electrical conductivity of potato would catch up with that of the fluid, alleviating the above current channeling effect. From the maps for the holding period, we can see that the temperature changed slowly, indicating a small heat transfer rate within the 2-phase systems.

Fluid-particulate heat transfer coefficient

Figures 6(a) and (b) present the calculated heat transfer coefficients (h_{fp}) over 5-min intervals during the holding period for the 2 samples. The results fall into the range of the literature values (Maesmans and others 1992) for natural convection conditions.

The effect of the fluid relative viscosity ("viscosity" is inappropriate per se, because CMC solutions exhibit non-Newtonian behavior) on h_{fp} was pondered. Generally, the relative viscosity of CMC solutions increases with the increasing CMC concentration and the decreasing temperature (Gomez-Diaz and Navaza 2002). Sample nr 2 had a higher interface heat transfer rate than sample nr 1 due to its lower viscosity and the larger temperature difference between the 2 phases. A similar trend for the 2 samples that can be observed from the figures is that the h_{fp} value decreased sharply during the first few min of the holding period and then leveled off. The physical explanation for this observation may be that fluid flow existed immediately after the ohmic heating power was disconnected, because the fluids were heated to nearly boiling (the fluid temperature reached about 95 °C). As time passed, the effect of the fluid flow faded out, resulting in smaller h_{fp} values. As the samples cooled, the relative viscosity of the fluids increased and the temperature difference between the 2 phases decreased, resulting in a smaller and less variable heat transfer coefficient. The observation of this viscosity effect is consistent with the literature (Maesmans and others 1992). Other factors, such as density, specific heat, and thermal conductivity of the potato, might also be function of temperature but were simplified as constants in this study. This simplification apparently affected the accuracy of the h_{fp} estimation. However, the temperature dependence of these properties is a rather weak function as shown in Rahman (1995). Simulation in MATLAB using 3515 J/kg K instead of 3795 J/kg K as the value of the potato specific heat for sample nr 1 resulted in an under-estimation of the h_{fp} values by less than 3 W/m^2·K.

It might be thought that the instantaneous values of the h_{fp} could be approached if we could acquire MRI temperature images at smaller time intervals. This would imply determining values of h_{fp} out of very small heat fluxes in the numerical simulation, corresponding to the incremental time stepping into which the domain is discretized by the numerical procedure. The resulting situation is similar to the difficulty of trying to solve Eq. 5 and 6 for small temperature gradients—if Δt or ΔT is very small, the error of determination of h_{fp} will be high. Moreover, a convergence may not be achieved for the iterative computation if the time interval is too small. Therefore, an increment of 5 min was used for both samples. The calculated h_{fp} values are thus the average heat transfer coefficients over the 5-min intervals. In most cases reported in the literature, temperature measurements at the center of a particle were used to calculate h_{fp} and the assumption of a well-described conduction heat transfer within the particle was required. In this study, the temperature profiles of nearly the entire domain of the particles were taken into consideration, resulting in a more reasonable estimate of h_{fp}.

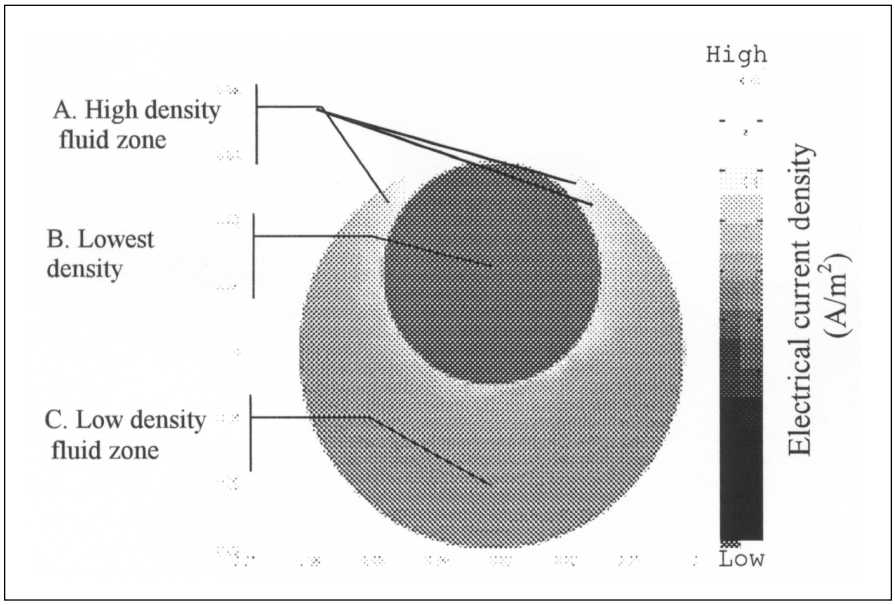

Figure 5—Simulation of electrical current density distribution using Laplace equation

Conclusions

TEMPERATURE MAPS OF OHMICALLY HEATED food systems can be obtained, without disconnecting the electrical heating power, using the PRF shift method. The processing algorithm of the PRF shift method can eliminate the noise induced by the electrical power. The observations from the temperature maps support the application of Laplace equation to model the electric field during ohmic heating.

The MRI temperature maps together with the numerical solutions to the Fourier's 2nd law can be used to estimate the time-dependent interface heat transfer coefficients during the holding period. With more knowledge about the electrical conductivity and its temperature dependence of the food materials, this procedure can easily be adapted to determine h_{fp} during the ohmic heating period. The calculated heat transfer coefficients ranges from 30 to 105 $W/m^2 \cdot K$, which is consistent with the literature values for natural convection. It was found that the heat transfer coefficients decreased sharply during the first few min of the holding period and then leveled off, decreasing only slightly. It was also observed that the sample with a lower fluid relative viscosity has a larger interface heat transfer coefficient comparing with the sample with a higher fluid relative viscosity.

References

Anantheswaran RC, Rao MA. 1985. Heat transfer to model non-Newtonian liquid foods in cans during end-over-end rotation. J Food Engin 4:1.

Awuah GB, Ramaswamy HS, Simpson BK, Smith JP. 1996. Fluid-to-particle convective heat transfer coefficient as evaluated in an aseptic processing holding tube simulator. J Food Proc Engin 19:241.

Azevedo ICA, Oliveira FAR, Drumond MCS. 1998. A study on the accuracy and precision of external mass transfer and diffusion coefficients jointly estimated from pseudo-experimental simulated data. Math Comp Simul 48(1):11-22.

Bhamidipati S, Singh RK. 1995. Determination of fluid-particle convection heat transfer coefficient. Trans ASAE 38(3):857-62.

de Alwis AAP, Fryer PJ. 1990. A finite element analysis of heat generation and transfer during ohmic heating of foods. Chem Engin Sci 45:1547-59.

de Alwis AAP, Fryer PJ. 1992. Operability of the ohmic heating process: electrical conductivity effects. J Food Engin 15(1):21-48.

Fryer PJ, de Alwis AAP, Koury E, Stapley AGF, Zhang L. 1993. Ohmic processing of solid-liquid mixtures: heat generation and convection effects. J Food Engin 18(2):101-25.

Gomez-Diaz D, Navaza JM. 2002. Rheological characterization of aqueous solutions of the food additive carboxymethyl cellulose. Electr J Environ Agric Food Chem 1(1):2002 (ISSN: 1579-4377).

Gratzek JP, Toledo RT. 1993. Solid food conductivity determination at high temperatures. J Food Sci 58(4):908.

Halden K, de Alwis AAP, Fryer PJ. 1990. Changes in the electrical conductivity of foods during ohmic heating. Int J Food Sci Technol 25(1):9-25.

Hindman JC. 1966. Proton resonance shift of water in the gas and liquid states. J Chem Phys 44:4582-92.

Hulbert GJ, Litchfield JB, Schmidt SJ. 1995. Temperature mapping in carrot using T_1 weighted magnetic resonance imaging. J Food Sci 60(4):780-5.

Ishihara Y, Calderon A, Watanabe H, Okamoto K, Suzuki Y, Kuroda K, Suzuki Yu. 1995. A precise and fast temperature mapping using water proton chemical shift. Magnet Reson Med 34:814-23.

Kim, HJ, Choi YM, Yang TCS, Taub IA, Tempest P, Skudder P, Tucker G, Parrott DL. 1996. Validation of ohmic heating for quality enhancement of food products. Food Technol 50(5):253-5, 257-61.

Maesmans G, Hendrickx M, Decordt S, Fransis A. 1992. Fluid-to-particle heat transfer coefficient determination of heterogeneous foods: a review. J Food Proc Pres 16:29-69.

Merson RL, Stoforos NG. 1990. Motion of spherical particles in axially rotating cans: effect on liquid-particle heat transfer. In: Spiess WEL, Schubert H, editors. Engineering and Food. Vol. 2. Amsterdam, The Netherlands: Elsevier. 160 p.

Muller N, Reiter RC. 1965. Temperature dependence of chemical shifts of protons in hydrogen bonds. J Chem Phys 42:3265-9.

Orangi S, Sastry SK, Li Q. 1998. A numerical investigation of electroconductive heating of solid-liquid mixtures. Int J Heat Mass Trans 41(14):2211-20.

Palaniappan S, Sastry SK. 1991a. Electrical conductivities of selected solid foods during ohmic heating. J Food Proc Engin 14(3):221-36.

Palaniappan S, Sastry SK. 1991b. Electrical conductivities of selected juices: influences of temperature, solid content, applied voltage, and particle size. J Food Proc Engin 14(3):247-60.

Rahman S. 1995. Food properties handbook. Boca Raton, Fla.: CRC Press.

Sastry SK, Li Q. 1996. Modeling the ohmic heating of foods. Food Technol 50(5):246-8.

Schrader GW, Litchfield JB, Schmidt SJ. 1992. Magnetic resonance imaging applications in the food industry. Food Technol 46(12):77-83.

Sun X, Schmidt SJ, Litchfield JB. 1994. Temperature mapping in a potato using half Fourier transform MRI of diffusion. J Food Proc Engin 17:423-37.

Ye X, Ruan R, Chen P, Chang K, Ning K, Taub I, Doona C. 2002. Accurate and fast temperature mapping during ohmic heating using PRF shift MRI thermometry. J Food Engin (Forthcoming).

MS 20020361 Submitted 6/12/02, Revised 1/8/03, Accepted 1/31/03, Received 2/3/03

Authors Ye, Ruan, and Chen are with the Dept. of Biosystems & Agricultural Engineering, Univ. of Minnesota, St. Paul, MN 55108. Authors Doona and Taub are with the US Army Natick RD&E

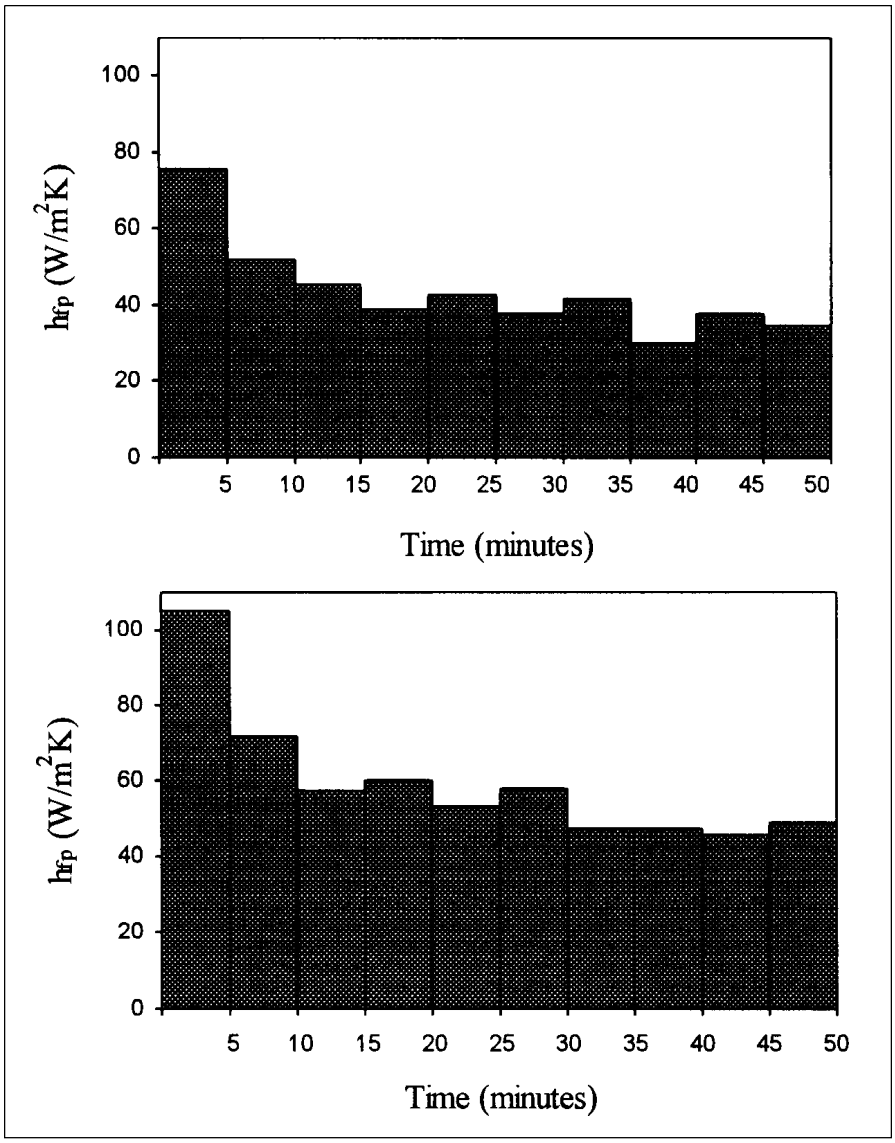

Figure 6—(a, top) Calculated heat transfer coefficients for sample nr 1; (b, bottom) calculated heat transfer coefficients for sample nr 2

JFS is available in searchable form at *www.ift.org*